Propagation in tunnels: experimental investigations and channel modeling in a wide frequency band for MIMO applications

J.M. Molina-Garcia-Pardo, M. Lienard, Pierre Degauque

Hindawi Publishing Corporation
EURASIP Journal on Wireless Communications and Networking
Volume 2009, Article ID 560571, 9 pages
doi:10.1155/2009/560571

Research Article

Propagation in Tunnels: Experimental Investigations and Channel Modeling in a Wide Frequency Band for MIMO Applications

J.-M. Molina-Garcia-Pardo,[1] M. Lienard,[2] and P. Degauque[2]

[1] *Departamento de Tecnología de la Información y la Comunicación, Technical University of Cartagena, 30202 Cartagena, Spain*
[2] *Télécommunications, Interférences et Compatibilité Electromagnétique (TELICE), Institut d'Electronique, Microélectronique et Nanotechnologie (IEMN), University of Lille, 59655 Villeneuve D'Ascq, France*

Correspondence should be addressed to J.-M. Molina-Garcia-Pardo, josemaria.molina@upct.es

Received 25 July 2008; Accepted 10 February 2009

Recommended by Jun-ichi Takada

The analysis of the electromagnetic field statistics in an arched tunnel is presented. The investigation is based on experimental data obtained during extensive measurement campaigns in a frequency band extending from 2.8 GHz up to 5 GHz and for a range varying between 50 m and 500 m. Simple channel models that can be used for simulating MIMO links are also proposed.

1. Introduction

Narrowband wireless communications in confined environments, such as tunnels, have been widely studied for years, and a lot of experimental results have been presented in the literature in environmental categories ranging from mine galleries and underground old quarries to road and railway tunnels [1–4].

However, in most cases, measurements dealt with channel characterization for few discrete frequencies, often around 900 MHz and 1800 MHz. For example, in [5, 6] Zhang et al. report statistical narrowband and wideband measurement results. In [7], results on planning of the Global System for Mobile Communication for Railway (GMS-R) are presented. In [8], simulations and measurements are also described in the same GSM frequency band. In [9], the prediction of received power in the out-of-zone of a dedicated short range communications (DSRC) system operating inside a typical arched highway tunnel is discussed, and in this case the channel impulse response was measured with a sounder at 5.2 GHz whose bandwidth is on the order of 100 MHz. Recently, in [10], measurement campaigns have been performed in underground mines in the 2–5 GHz band but the results cannot be extrapolated to road and railway tunnels since the topology is quite different. In a mine gallery, roughness is very important, the typical width is 3 m, the geometry of the cross-section is not well defined and lastly, there are often many changes in the tunnel direction.

Furthermore, to increase the channel capacity in tunnels, space diversity both at the mobile and at the fixed base station can be introduced. However, good performances of multiple input multiple output (MIMO) techniques can be obtained under the condition of a small correlation between paths relating each transmitting and receiving antennas. This decorrelation is usually ensured by the multiple reflections on randomly distributed obstacles, giving often rise to a wide spread in the direction of arrival of the rays. On the contrary, a tunnel plays the role of an oversized waveguide and decorrelation can be due to the superposition of the numerous hybrid modes supported by the structure [11]. Experimental results at 900 MHz for a $(4, 4)$ MIMO configuration, are described in [12]. This paper shows that the antenna arrays must be put in the transverse plane of the tunnel to minimize the coupling between elements.

The objective of this work is thus to extend the previous approaches by investigating the statistics of the electric field

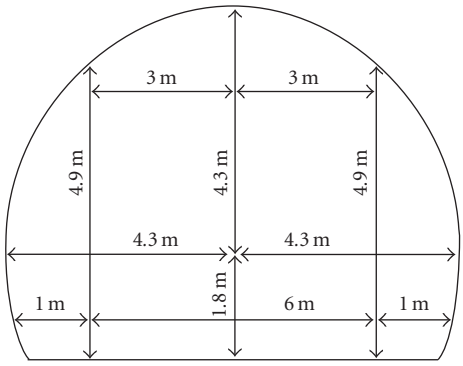

Figure 1: Cross-section of the tunnel.

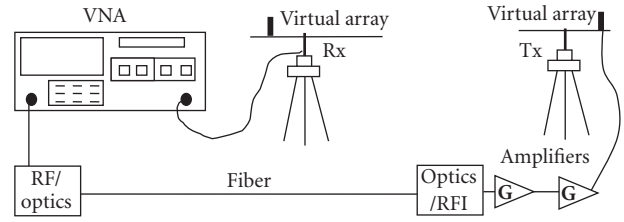

Figure 2: Principle of the channel sounder setup.

distribution in the 2.8–5 GHz frequency range in a tunnel environment for MIMO applications. Empirical formulas based on the experimental results are also proposed.

We proceed in two steps: (1) determination of the mean path loss and of the statistical distribution of the average field which can be received by the various antennas of an MIMO system. This first approach can thus be used to determine the average power related to the **H** matrix of an MIMO link, (2) field distribution and correlation in a transverse plane.

The paper is distributed as follows. Section 2 explains the experiments in detail and more specifically the environment and methodology of the measurements that has been followed. Section 3 investigates path loss and axial correlation while, in Section 4, field statistics in the transverse plane are analyzed. Section 5 deals with the transverse spatial correlation and Section 6 presents the principle of modeling the MIMO channel and gives an example of application. Finally, Section 7 summarizes the contributions of the present work and gives conclusions.

2. Environment, Measurement Equipment, and Methodology

2.1. Description of the Environment. The measurement campaign was performed in a 2-way tunnel, situated in the French Massif Central mountains. This straight tunnel, 3.4 km long, has a semicircular shape, as shown in Figure 1. The diameter of the cylindrical part is 8.6 m and the maximum height of the tunnel is 6.1 m. The tunnel was empty with no pipes, cables, or lights. However, every 100 m there are small safety zones, 1 m wide and few meters long, where an extinguisher is hung. It is difficult to estimate the roughness accurately but it is on the order of a centimetre. The tunnel was closed to traffic during the experiments, to make measurements in stationary conditions.

2.2. Measurement Equipment. Since we want to explore the channel response in a very wide frequency band (2.8–5 GHz), we have chosen to make measurements in the frequency domain rather than in the time domain, so as to get better accurate results. The complex channel transfer function between the transmitting (Tx) and receiving (Rx) antennas has thus been obtained by measuring the S_{21} parameter with a vector network analyzer (VNA Agilent E5071B). The Rx antenna is directly connected to one port of the VNA using a low attenuation coaxial cable, 4 m long, a 30 dB low-noise amplifier being inserted or not, depending on the received power. Using a coaxial cable to connect the Tx antenna to the other port of the VNA would lead to prohibitive attenuation, the maximum distance between Tx and Rx being 500 m. The signal of the Tx port of the VNA is thus converted to an optical signal which is sent through fibre optics, converted back to radio frequency and amplified. The signal feeding the vertical biconical transmitting (Tx) antenna has a power of 1 W. The phase stability of the fibre optics link has been checked and the calibration of the VNA takes amplifiers, cables, and optic coupler into account. The block diagram of the channel sounder is depicted in Figure 2.

The wideband biconical antennas (Electrometrics EM-6116) used in this experiment have nearly a flat gain, between 2 and 10 GHz. Indeed, the frequency response of the two antennas has been measured in an anechoic chamber, and the variation of the antenna gain was found to be less than 2 dB in our frequency range. Nevertheless, we have subtracted the antenna effect in the measurements, as it will be explained in Section 3.

It must also be emphasized that, in general, the radiation pattern of wideband antennas is also frequency dependent. This is not a critical point in our case since, in a tunnel, only waves impinging the tunnel walls with a grazing angle of incidence contribute to the total received power significantly. This means that, whatever the frequency, the angular spread of the received rays remains much smaller than the 3 dB beam width of the main antenna lobe in the E plane, equal to about 80°, the antenna being nearly omnidirectional in the H plane.

Since the channel transfer function may also strongly depend on the position of the antennas in the transverse plane of the tunnel, both Tx and Rx antennas were mounted on rails. The position mechanical systems are remote controlled, optic fibres connecting the step by step motors to the control unit.

2.3. Methodology. The channel frequency response has been measured for 1601 frequency points, equally spaced between 2.8 and 5 GHz, leading to a frequency step of 1.37 MHz.

The rails supporting the Tx and Rx antennas were put at a height of 1 m and centred on the same lane of this 2-lane tunnel. For each successive axial distance d, both

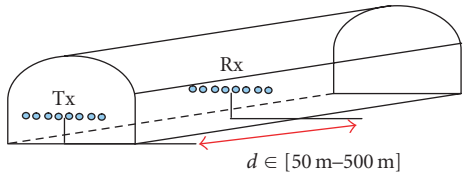

Figure 3: Configuration of the wideband MIMO measurements.

Table 1: Equipment characteristics and measurement parameters.

Frequency band	2.8–5 GHz
Number of frequency points	1601
Antenna	Biconical antenna (Electrometrics EM-6116)
Transmitter power	20 dBm
Dynamic range	>100 dB
Position in the transverse plane	12 positions every 3 cm ($\lambda/2$ at 5 GHz)
Positions along the longitudinal axis	From 50 m to 202 m every 4 m From 202 m to 500 m every 6 m
Number of acquisitions at each position	5

the Tx and Rx antennas were moved in the transverse plane on a distance of 33 cm, with a spatial step of 3 cm, corresponding to half a wavelength at 5 GHz. A $(12, 12)$ transfer matrix is thus obtained, the configuration of the measurements being schematically described in Figrue 3. Fine spatial sampling was chosen for measurements in the transverse plane because, as recalled in the introduction, antenna arrays for MIMO applications have to be put in this plane to minimize correlation between array elements.

Due to the limited time available for such an experiment and to operational constraints, it was not possible to extensively repeat such measurements for very small steps along the tunnel axis. In the experiments described in this paper, the axial step was chosen equal to 4 m when $50\,\text{m} < d < 202\,\text{m}$ and to 6 m when $202\,\text{m} < d < 500\,\text{m}$. This is not critical because we are interested, in the axial direction, by the mean path loss and by the large-scale fluctuation of the average power received in the transverse plane. At each Tx and Rx position, 5 successive recordings of field variation versus frequency are stored and averaged.

It must be noted that in the case of a single input single output (SISO) link, a number of papers have already been published on the small-scale variation of a narrowband signal along the tunnel axis. For example, [13] describes results of experiments carried out in a wide tunnel at a frequency of 900 MHz. A summary of the measurement parameters and equipment characteristics is summarized in Table 1.

3. Path Loss and Correlation Along the Longitudinal Axis

3.1. Path Loss. The path loss is deduced from the measurement of the $S_{21}(f, d)$ scattering parameter. However, as briefly mentioned in the previous section, it can be more interesting to subtract the effects of the variation of the antenna characteristics with frequency by introducing a correction factor $C(f)$. We have thus made preliminary measurements by putting the two biconical antennas, 1 m apart, in an anechoic room. Let $S_{21}^{\text{anech}}(f)$ be the scattering parameter measured in this configuration. The correction factor is thus given by $C(f) = |S_{21}^{\text{anech}}(f)| - \langle |S_{21}^{\text{anech}}(f)| \rangle$, where $\langle x \rangle$ means the average of x over the frequency band.

The path loss in tunnel, taking this correction into account, is given by

$$\text{PL}(f, d) = -20 \cdot \log_{10}(|S_{21}(f, d)|) - (-20 \cdot \log_{10} C(f)). \tag{1}$$

Figure 4 shows the variation of $\text{PL}(f, d)$ versus frequency, for $d = 50\,\text{m}$. The fluctuation of the field amplitude is due to the combination in phase or out of phase of the various modes excited by the transmitting antenna, the phase of the propagation constant depending on frequency but also on the order of the hybrid modes propagating in the tunnel. To extract the variation of the mean path loss versus frequency, it is interesting to average such curves, obtained at any distance d, for the various transverse positions of the antennas. Furthermore, one can also average over few frequencies, considering a frequency bandwidth smaller than the channel coherence bandwidth. In this example, the coherence bandwidth being on the order of 10 MHz, $\text{PL}(f, d)$ was averaged over 7 frequencies around f, the frequency step being 1.37 MHz, and over the 144 successive combinations of the transverse positions of the Tx and Rx antennas. The average value $\langle \text{PL}(f, d) \rangle$ is also plotted in Figure 4.

The curves "measurements" in Figure 5 represent the variation of $\langle \text{PL}(f, d) \rangle$ versus axial distance at 3 and 5 GHz. The path loss, at 3 GHz, corresponding to free-space conditions, has been also plotted. We see that, in this frequency range, the path loss is only slightly dependent on frequency.

To deduce from these curves a simple theoretical model of the mean path loss $\overline{\text{PL}}(f, d)$, these curves must be smoothed again by introducing a running mean over the axial distance. To get a very simple approximate analytical expression of $\overline{\text{PL}}(f, d)$, it is assumed that $\overline{\text{PL}}(f, d)$ is the product of two functions, one depending on f and one depending on d [14].

Furthermore, it is usually expressed in terms of two path loss exponents, $n_{\text{PL}_0\text{-}f}$ and $n_{\text{PL}_0\text{-}d}$ which indicate the rate at which the path loss decreases with frequency and distance, respectively, [15]. This leads to

$$\begin{aligned}\overline{\text{PL}}(f, d) = {} & (\text{PL}_0 + 10 \cdot n_{\text{PL}_0\text{-}f} \log_{10}(f(\text{GHz}))) \\ & + 10 n_{\text{PL}_0\text{-}d} \log_{10}(d).\end{aligned} \tag{2}$$

The constant PL_0 and the path loss exponents have been determined by minimizing the mean square error between

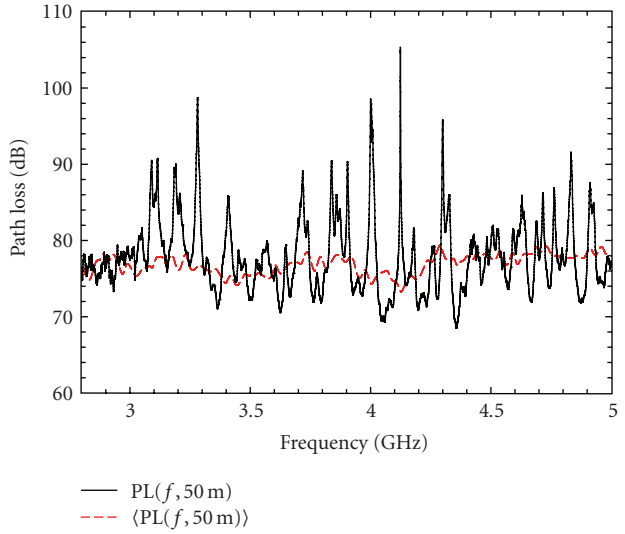

FIGURE 4: Path loss PL(f,d) between two antennas for $d = 50$ m and path loss $\langle \mathrm{PL}(f,d)\rangle$ averaged over the transverse positions of the antennas and over 7 frequencies in a 10 MHz band.

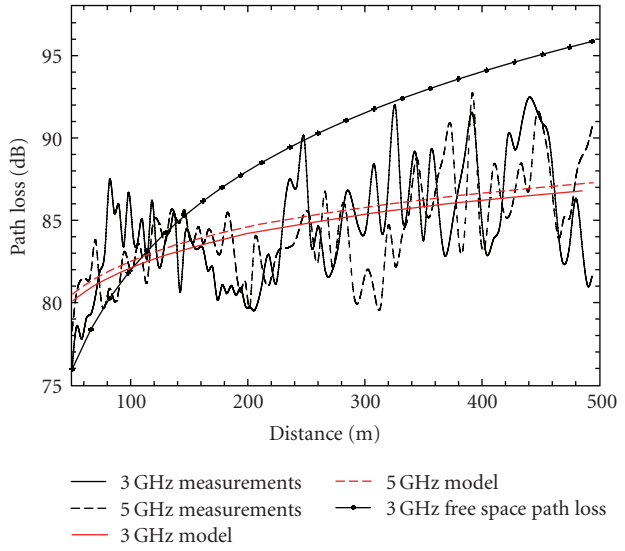

FIGURE 5: Average path loss (curves "measurements") and mean path loss deduced from the model (curves "model") at 3 and 5 GHz.

the measurements and the model. The following values were found: $\mathrm{PL}_0 = 86$ dB, $n_{\mathrm{PL}_0 - f} = 0.82$, and $n_{\mathrm{PL}_0 - d} = 0.57$. The corresponding curves for 3 and 5 GHz have also been plotted in Figure 5. It must be outlined that all these values were deduced from measurements between 50 and 500 m and consequently, they are valid only in this range of axial distance.

It can be interesting to compare this value of $n_{\mathrm{PL}_0 - d}$ to those already published in the literature and corresponding to attenuation factors measured for ultra-wideband systems in indoor environments. However, in this case, the range is much smaller, typically below 50 m. In line of sight (LOS) conditions, values from 1.3 to 1.7 were reported by [16, 17],

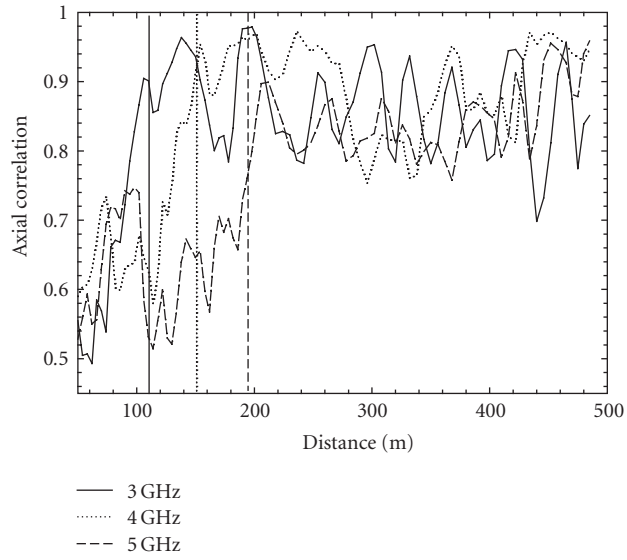

FIGURE 6: Axial correlation between receiving arrays 4 m (for 50 m $< d <$ 202 m) or 6 m (for 202 m $< d <$ 500 m) apart for three frequencies and their corresponding breakpoints.

while for non-LOS, $n_{\mathrm{PL}_0 - d}$ may reach 2 to 4 as mentioned in [18, 19]. The small value that we have obtained comes from the guiding effect of the tunnel.

The comparison between $\langle \mathrm{PL}(f,d)\rangle$ and the predicted path loss $\overline{\mathrm{PL}}(f,d)$ shows that the difference in their values is characterized by a standard deviation $\sigma_{\mathrm{PL}} = 2.7$ dB. $\langle \mathrm{PL}(f,d)\rangle$ can thus be modeled by (2) and by adding a random variable $X_{\sigma_{\mathrm{PL}}}$ with zero mean and standard deviation σ_{PL}:

$$\langle \mathrm{PL}(f,d)\rangle_{\mathrm{model}} = \overline{\mathrm{PL}}(f,d) + X_{\sigma_{\mathrm{PL}}}. \quad (3)$$

3.2. Axial Correlation. One can expect that the variation of the average received power between one transverse plane and another will depend on the distance d, high-order propagating modes suffering important attenuation at large distances. To study this point, we have calculated, for a given frequency, the amplitude ρ_{axial} of the complex correlation coefficient between the (12, 12) transfer matrix elements measured at a distance d and the matrix elements measured at the distance $d + \Delta d$, d varying between 50 m and 500 m. Let us recall that the step Δd is equal 4 m while 50 m $< d <$ 202 m and 6 m when 202 m $< d <$ 500 m.

Curves in Figure 6 give the variation of ρ_{axial} for three frequencies: 3, 4, and 5 GHz. As one can expect from the modal theory, the correlation is an increasing function of distance. At 3 GHz, for example, the correlation between 2 receiving arrays, 4 m apart, varies from 0.6 at 50 m, to reach an average value of 0.9 at a distance of 200 m. If we now compare results obtained at 3 and 5 GHz, we see that the correlation increases less rapidly at 5 GHz, because high-order modes suffer less attenuation. By examining the shape of these curves, we observe two regions: the first one, at short distance from the transmitter, where the correlation increases nearly linearly, and the other where the average value of the

correlation does not vary appreciably. A two-slope model seems thus well suited to fit the average variation of the correlation function.

In Figure 6, the three vertical lines correspond to the positions of the breakpoint between the two slopes, for the three frequencies, respectively. This breakpoint thus occurs at distance $d_{\text{breakpoint\_axial}}$ from the transmitter and by plotting all curves for frequencies between 2.8 and 5 GHz, the following empirical formula giving has been obtained:

$$10\log_{10}(d_{\text{breakpoint\_axial}}) = 16.8 + 1.2f\ (\text{GHz}). \tag{4}$$

At the breakpoint and beyond this distance, the average correlation between the fields received by the array elements, 6 m apart, is equal to $\rho_{\text{breakpoint}} = 0.88$, with a standard deviation $\sigma_{\rho\_\text{axial}} = 0.06$, this result remaining valid in all the frequency range. In the first zone, that is, for $d < d_{\text{breakpoint\_axial}}$, the average variation of ρ_{axial} is modelled by

$$\langle\rho_{\text{axial}}\rangle = \rho_{\text{breakpoint}} + 0.06(d_{\text{breakpoint\_axial}} - d) \tag{5}$$

the standard deviation $\sigma_{\rho\_\text{axial}}$ being also equal to 0.06.

This leads to the following expression for modeling the variation of the correlation coefficient along the tunnel axis:

$$\rho_{\text{axial,model}} = \langle\rho_{\text{axial}}\rangle + X_{\rho\_\text{axial}}. \tag{6}$$

4. Field Distribution in the Transverse Plane

4.1. Field Distribution Function. In the transverse plane, the field distribution was first studied by considering, for a given axial distance d, the 12×12 possible combinations of the Tx and Rx antennas, and 7 close frequencies, within a 10 MHz band, as earlier explained. This has been done for various frequency bands between 2.8 and 5 GHz. We have compared the measured data to those given by a Rayleigh, Weibull, Rician, Nakagami and Lognormal distribution, and then using the Kolmogorov-Smirnov [20] test to decide what distribution best fits the experimental results. A Rice distribution appears to be the optimum one, whatever the frequency. The mathematical expression of its probability density function (PDF) is given by

$$f(x \mid \nu, \sigma_{\text{RICE}}) = \frac{x}{\sigma^2_{\text{RICE}}} \exp\left(\frac{-(x^2+\nu^2)}{2\sigma^2_{\text{RICE}}}\right) I_0\left(\frac{x\nu}{\sigma^2_{\text{RICE}}}\right). \tag{7}$$

In this formula, $I_0(\cdot)$ is the modified Bessel function of the first kind with order zero and ν and σ_{RICE} are parameters to be adjusted. The first order moment is expressed as

$$E(x) = \sqrt{\frac{\pi}{2}}\sigma_{\text{RICE}} L_{1/2}\left(-\frac{\nu^2}{2\sigma^2_{\text{RICE}}}\right) = \sqrt{\frac{\pi}{2}}\sigma_{\text{RICE}} L_{1/2}(-K), \tag{8}$$

$L_{1/2}$ being a Laguerre polynomial.

Before explaining how the two parameters of the Rice distribution have been found, let us recall that, in the mobile communication area, a Rice distribution usually characterizes the field distribution in line of sight (LOS) conditions and in presence of a multipath propagation. Usually a K factor is introduced and defined as the ratio of signal power in dominant component, corresponding to the power of the direct ray, over the scattered, reflected power. One can follow the same approach by defining a K factor in a given receiving zone which is, in our case, defined by the segment 33 cm long in the transverse plane of the tunnel, along which measurements were carried out.

4.2. Ricean K Factor. Knowing the (12, 12) matrix whose elements are the S_{21} complex values for successive positions of the Tx and Rx antennas in the transverse plane, one can calculate K at a distance d and a frequency f, from the following expression:

$$K = \frac{|\langle S_{21}\rangle|^2}{\left\langle |S_{21} - \langle S_{21}\rangle|^2 \right\rangle}. \tag{9}$$

It must be clearly outlined that, in a tunnel, the K factor cannot be easily interpreted. Indeed, there is no contribution of random components to the received power, the position of the 4 reflecting walls being invariant. K could be related to richness in terms of propagation modes having a significant power in the receiving transverse plane, a high number of modes giving rise to a high fluctuating field. However, quantifying the relationship between K and mode richness is not easy since the field fluctuation depends not only on the amplitude of the modes but also on their relative phase velocity. In a tunnel, one can conclude that K just gives an indication on the relative range of variation of the received power in a given zone.

Curves in Figure 7 have been plotted for 2 frequencies: 3 and 5 GHz. In the transverse zone of investigation (33 cm), for distances smaller than 200 m, the K factor is below -15 dB, which means that the received power strongly varies in the transverse plan, nearly following a Rayleigh distribution. However, K increases with distance and reaches 0 dB or more beyond 400 m, the constant part of the distribution becoming equal to or greater than the random part.

This increase of K is due to the fact that the contribution of high-order modes becomes less important leading to less fluctuation of the transverse field. The same interpretation based on the modes can be made to interpret the influence of frequency on the K values. The variation of K is of course related to the variation of the correlation coefficient along the tunnel axis, as described in the previous section.

By following the same approach as for the path loss, described in Section 3, and thus by averaging K over groups of 7 frequencies and over 144 successive combinations of the transverse positions of the transverse positions of the Tx and Rx antennas, an empirical expression of the average K factor in terms of frequency and distance can be found. It is given by

$$\overline{K} = (K_0 + 10 \cdot n_{K_0}\log_{10}(f(\text{GHz}))) + 10 \cdot (n_0 + 10 \cdot n_{n_0}\log_{10}(f(\text{GHz})))\log_{10}(d). \tag{10}$$

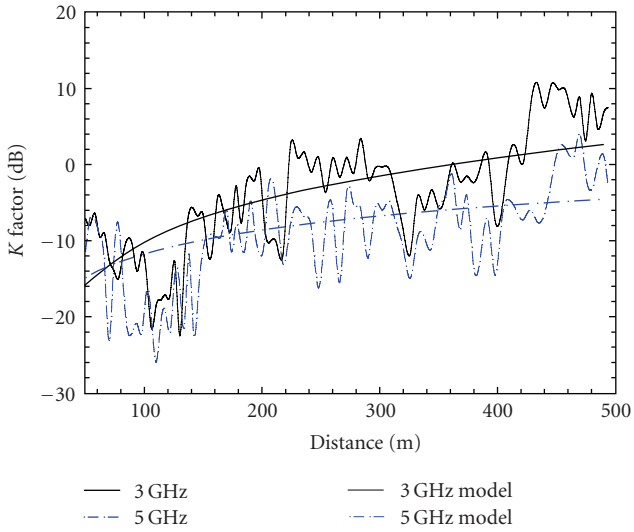

Figure 7: Variation of the K factor at 3 and 5 GHz, versus distance, and deduced from measurements. Its average variation calculated from an empirical mathematical expression is also plotted.

Table 2: Parameters to be introduced in (10) for modeling the variation of the K factor.

	K_0	n_{K_0}	n_0	n_{n_0}	σ_K
Values	−79	6.73	3.6	−0.37	4.9

The best fit between the results given by (10) and those extracted from the measurements was obtained for the values of the parameters given in Table 2. The standard deviation between (10) and the measured K is given by σ_K.

The curves labelled "model" in Figure 7 have been obtained by applying (10) and the above values for the parameters.

Let X be a random variable of zero mean. To completely describe the model, we can add to $\overline{K}$ such a random variable with a standard deviation of σ_K and labeled X_{σ_K}:

$$K_{\text{model}} = \overline{K} + X_{\sigma_K}. \tag{11}$$

4.3. Determination of the Ricean Parameters and Modeling of the Field Variation in the Transverse Plane. $\overline{K}$ is related to the field distribution parameters of the Rice distribution by

$$\overline{K} = \frac{\nu^2}{2\sigma^2_{\text{RICE}}}. \tag{12}$$

The mean value of $\overline{K}$ is deduced from (10) for a given frequency and distance, and by assuming a mean value of 1 of the amplitude of the field distribution $E(x) = 1$, the field distribution parameters ν and σ_{RICE} can be calculated. Note that mean value of the field would be determined by the large-scale fading, and fast variations around the mean value by the Rice distribution. Therefore, σ_{RICE} can be computed using (8) and (12):

$$\sigma_{\text{RICE}} = \sqrt{\frac{2}{\pi}} \frac{1}{L_{1/2}(-\overline{K})}. \tag{13}$$

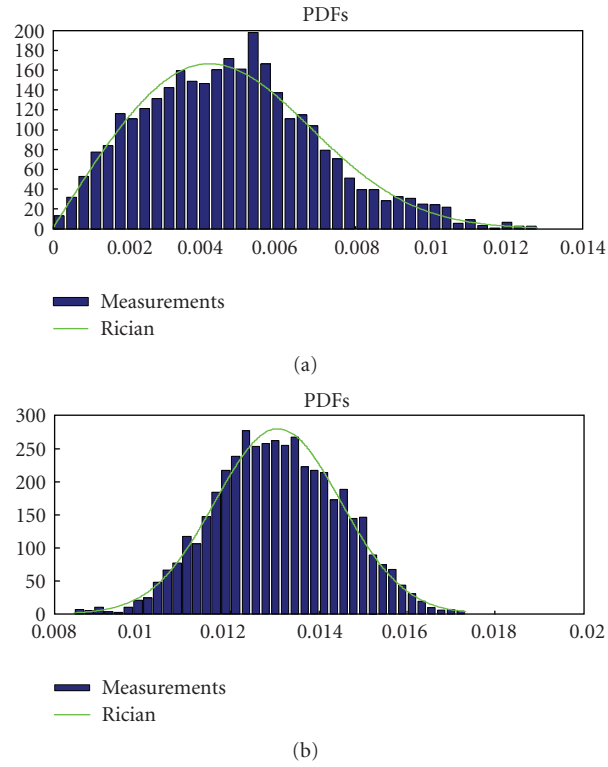

Figure 8: PDFs of the field amplitude in a transverse plane either deduced from measurements or calculated assuming a Rice distribution: (a) $d = 50$ m and $f = 5$ GHz, (b) $d = 500$ m and $f = 3$ GHz.

By knowing σ_{RICE}, ν is immediately deduced from (12). As an example, curves (a) and (b) in Figure 8 compare the PDFs deduced from the measurements to those assuming a Rice distribution, for $d = 50$ m and $f = 5$ GHz, and $d = 500$ m and $f = 3$ GHz, respectively. We see the rather good agreement between measurements and the empirical formulation; the confidence level of the Smirnoff-Kolmogorov test remaining below 0.05.

5. Transverse Spatial Correlation

The knowledge of the spatial correlation in the transverse plane is of special interest for MIMO systems. It is assumed, for simplicity, that the correlations at the transmitter and at the receiver are separable [21]. Furthermore, since the Rx and Tx antenna arrays are situated in the same transverse zone of the tunnel, one can expect that the correlation statistics are the same for the Tx site and for the Rx site and thus, in the following, they are not differentiated.

For each axial distance d, and for each frequency f, the amplitude of the complex correlation function ρ_{trans} was deduced from the 12×12 channel matrix, whose elements are associated to the successive positions of the Tx and Rx antennas in the transverse plane. Let s be the spacing between two receiving points. Figure 9 shows, for $f = 3$ GHz, the variation of ρ_{trans} versus the axial distanceand for different values of s: 3, 9, 21, and 33 cm.

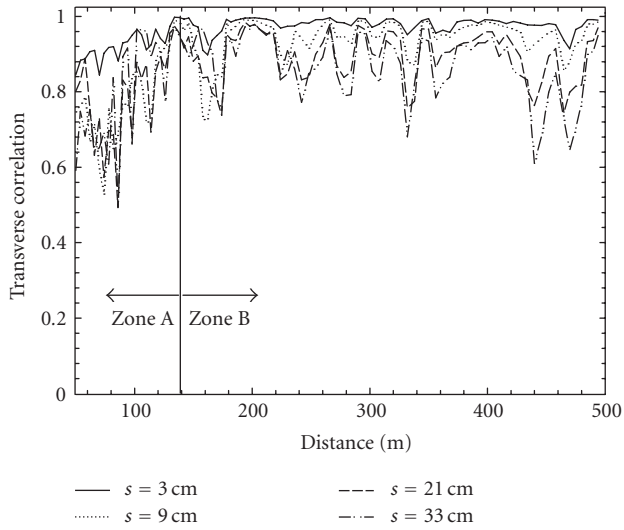

Figure 9: Transverse correlation at 3 GHz versus axial distance and for different spacing in the transverse plane.

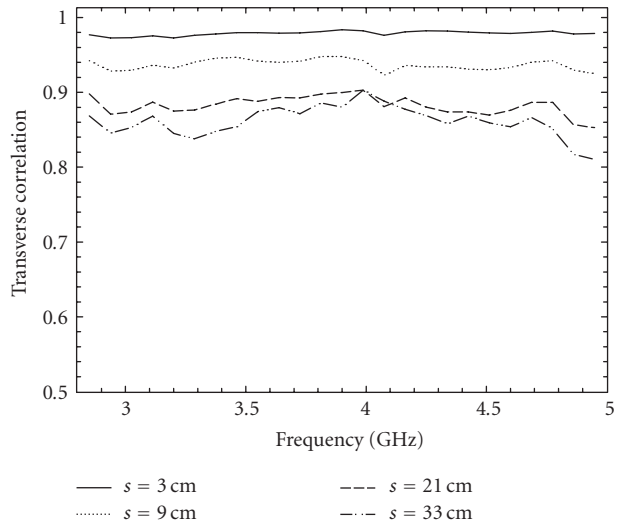

Figure 10: Average correlation in zone B, versus frequency, and for four antenna spacing.

ρ_{trans} is of course a decreasing function of the antenna spacing. Furthermore, for a given spacing, the correlation in the transverse plane increases when the axial distance increases, at least until the end of a zone, named A in Figure 9, occurring at a point called "breakpoint trans." This remark is connected to the comments made in Section 4 concerning the axial correlation, where we have outlined that, when the axial distance increases, the high-order modes are more and more attenuated, leading to a less fluctuating electromagnetic field. Beyond the "breakpoint trans" (zone B in Figure 9), ρ_{trans} keeps an average high value, even if local decreases are observed. The local decreases can be explained by the field pattern in the transverse plane of the tunnel. Indeed, this pattern does not present translation symmetry since it results from the combining of many modes, both in amplitude and in phase.

By analyzing results in the whole frequency range, it appears that the width of zone A slightly increases with frequency, as it occurred in the case of the longitudinal correlation (Section 4). Again, using all measured frequencies, an empirical formula giving the position of the "breakpoint_trans" point is given by

$$10\log_{10}\left(d_{\text{breakpoint\_trans}}\right) = 16 + 1.7f\,(\text{GHz}). \tag{14}$$

In zone B, one can calculate the mean value $\rho_{\text{trans}}(s, \text{zone } B, f)$ by averaging $\rho_{\text{trans}}(s, d, f)$ over the axial distance d. The results are the curves plotted in Figure 10, versus frequency and for different values of s: 3, 9, 21, and 33 cm.

It appears that $\rho_{\text{trans}}(s, \text{zone } B, f)$ is nearly frequency independent and that an empirical formula fitting the experimental results can be obtained:

$$\rho_{\text{trans}}(s, \text{zone } B) = 0.98 - 0.0042s\,(\text{cm}). \tag{15}$$

The difference between (15) and the measured correlation is a random variable of zero mean and standard deviation $\sigma_{\rho\_\text{trans}}$:

$$\sigma_{\rho\_\text{trans}}(s, \text{zone } B) = 0.02 + 0.0025s\,(\text{cm}). \tag{16}$$

The modeling of the ρ_{trans} in zone A assumes an average linear variation with distance. The adequate formula in this zone is

$$\rho_{\text{trans}}(s, d, f) = \rho_{\text{trans}}(s, \text{zone } B) + 0.04\left(d_{\text{breakpoint\_trans}} - d\right). \tag{17}$$

In this formula, the implicit dependence on frequency comes from the value of $d_{\text{breakpoint\_trans}}$. The standard deviation around this value is nearly frequency independent and is modeled by

$$\sigma_{\rho_{\text{trans}}}(s) = 0.0324 + 0.0033s\,(\text{cm}). \tag{18}$$

Finally, for a given antenna spacing, the correlation between two antenna elements is modeled by

$$\rho_{\text{trans,model}} = \rho_{\text{trans}} + X_{\sigma\rho\_\text{trans}}. \tag{19}$$

6. Full Model

The previous sections have proposed empirical formulas, based on experimental results, to model the path loss and the field fluctuation and correlation in a transverse plane. These formulas can be applied to randomly generate the transfer matrices $\mathbf{H}$ of an MIMO link in a straight tunnel having an arched cross-section, which is the shape of most road and railway tunnels. The transmitting and receiving arrays are supposed to be linear arrays, whose axes are horizontal and situated in the transverse plane of the tunnel, this configuration being quite usual. An approach based on the Kronecker model [21] was chosen for its simplicity.

To determine the various elements of **H**, the following steps can be followed:

(1) define the system parameters, such as frequency, distance between the transmitter and the receiver, number of array elements at the transmitter and at the receiver, element spacing and number of snapshots, corresponding to the number of realizations to be simulated;

(2) determine a value for the path loss $\mathrm{PL}(f,d)$ using (3);

(3) compute a K factor from (11). We recall that in (3) and in (11), the value given by the model is the sum of two terms: a deterministic one plus a random variable whose standard deviation is known;

(4) knowing K and $\mathrm{PL}(f,d)$, the elements of a $\mathbf{G}_{\mathrm{trans}}$ matrix, having the same size as **H**, are randomly chosen in a normalized Ricean distribution;

(5) as mentioned in Section 4, it was assumed that the correlations between either the transmitting elements or the receiving elements follow the same distribution. The terms of the correlation matrices at the transmitting and receiving sites, R_{Rx} and R_{Tx}, are thus deduced from (19).

The Kronecker model leads to

$$\mathbf{H} = \mathrm{PL}(f,d)\mathbf{R}_{\mathrm{Rx}}^{1/2}\mathbf{G}_{\mathrm{trans}}\left(\mathbf{R}_{\mathrm{Tx}}^{1/2}\right)^{T}. \tag{20}$$

To give an example of application of this formula, let us consider a 4×4 MIMO system at 4 GHz, an array element spacing of 0.8λ (6 cm at 4 GHz) and a distance d between the transmitter and the receiver of 250 m.

The channel capacity of a MIMO system for a given channel realization **H** can be computed as [22]

$$C = \log_2\left(\det\left|\mathbf{I}_N + \frac{\mathrm{SNR}}{M}\mathbf{H}\mathbf{H}^{\dagger}\right|\right), \tag{21}$$

where $\mathbf{I}_N$ is the $N \times N$ identity matrix, $(\,)^{\dagger}$ is the transpose conjugate operation and SNR is the signal-to-noise ratio at the receiver. The channel capacity C was calculated by assuming a fixed SNR equal to 10 dB. A constant SNR was chosen because we want to emphasize the influence of correlation and field distribution in the transverse plane. To compute the capacity assuming a fixed transmitting power, the contribution of the path loss must be added, which is straightforward.

The model was applied by considering 1000 realizations and the cumulative probability density function of the capacity is plotted in Figure 11 (curve "model"). To be able to compare this distribution to experimental results, a large number of measured values are needed. To increase this number we have thus calculated the capacity not only at 4 GHz, but also for all frequencies within a 100 MHz band around 4 GHz. We see in Figure 11, the rather good agreement between results deduced from the experiments (curve "measurements") and those given by the model.

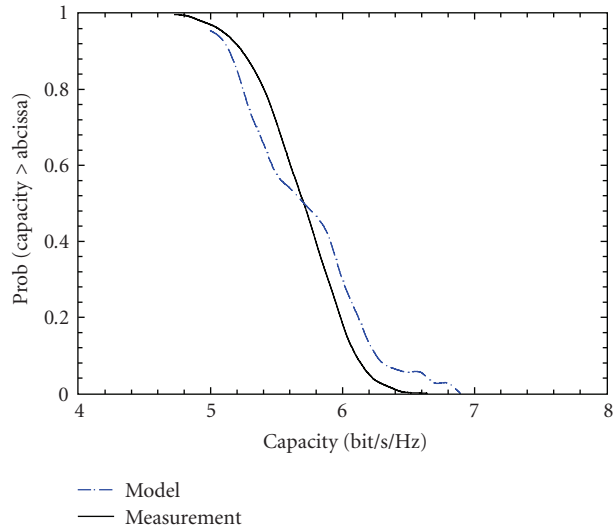

Figure 11: Application of the MIMO model for a 4×4 MIMO system, for a frequency of 4 GHz and for a distance of 250 m.

7. Conclusion

The statistics of the electromagnetic field variation in a tunnel has been deduced from measurements made in an arched tunnel, which is the usual shape of road and railway tunnels, and in a frequency range extending from 2.8 to 5 GHz. Both the methodology of the experiments and the analysis were aimed at predicting the performance of an MIMO link in a wide frequency band.

It was shown, by subtracting the antenna effect, that the path loss is not strongly dependent on frequency and that the attenuation constant keeps small values, the tunnel behaving as a low-loss guiding structure. Along the investigated transverse axis of the tunnel, over 33 cm long, the small-scale fading follows a Ricean distribution. However, for distances between the transmitting and receiving antennas up to 200 m, the$K$ factor is below -15 dB, meaning that the field is nearly Rayleigh distributed. It also appeared that K is an increasing function of distance, reaching 0 dB at about 400 m.

Empirical formulas to model the main propagation characteristics were proposed and applied to generate transfer matrices of an MIMO link.

Acknowledgments

This work has been supported by the European FEDER funds, the Region Nord-Pas de Calais, and the French ministry of research, in the frame of the CISIT project.

References

[1] Y. Yamaguchi, T. Abe, and T. Sekiguchi, "Radio wave propagation loss in the VHF to microwave region due to vehicles in tunnels," *IEEE Transactions on Electromagnetic Compatibility*, vol. 13, no. 1, pp. 87–91, 1989.

[2] M. Lienard and P. Degauque, "Natural wave propagation in mine environments," *IEEE Transactions on Antennas and Propagation*, vol. 48, no. 9, pp. 1326–1339, 2000.

[3] D. Didascalou, J. Maurer, and W. Wiesbeck, "Subway tunnel guided electromagnetic wave propagation at mobile communications frequencies," *IEEE Transactions on Antennas and Propagation*, vol. 49, no. 11, pp. 1590–1596, 2001.

[4] X. Yang and Y. Lu, "Research on propagation characteristics of millimeter wave in tunnels," *International Journal of Infrared and Millimeter Waves*, vol. 28, no. 10, pp. 901–909, 2007.

[5] Y. P. Zhang and Y. Hwang, "Characterization of UHF radio propagation channels in tunnel environments for microcellular and personal communications," *IEEE Transactions on Vehicular Technology*, vol. 47, no. 1, pp. 283–296, 1998.

[6] Y. P. Zhang, G. X. Zheng, and J. H. Sheng, "Radio propagation at 900 MHz in underground coal mines," *IEEE Transactions on Antennas and Propagation*, vol. 49, no. 5, pp. 757–762, 2001.

[7] C. Briso-Rodriguez, J. M. Cruz, and J. I. Alonso, "Measurements and modeling of distributed antenna systems in railway tunnels," *IEEE Transactions on Vehicular Technology*, vol. 56, no. 5, part 2, pp. 2870–2879, 2007.

[8] T.-S. Wang and C.-F. Yang, "Simulations and measurements of wave propagations in curved road tunnels for signals from GSM base stations," *IEEE Transactions on Antennas and Propagation*, vol. 54, no. 9, pp. 2577–2584, 2006.

[9] G. S. Ching, M. Ghoraishi, N. Lertsirisopon, et al., "Analysis of DSRC service over-reach inside an arched tunnel," *IEEE Journal on Selected Areas in Communications*, vol. 25, no. 8, pp. 1517–1525, 2007.

[10] M. Boutin, A. Benzakour, C. L. Despins, and S. Affes, "Radio wave characterization and modeling in underground mine tunnels," *IEEE Transactions on Antennas and Propagation*, vol. 56, no. 2, pp. 540–549, 2008.

[11] J.-M. Molina-Garcia-Pardo, M. Lienard, P. Degauque, D. G. Dudley, and L. Juan-Llàcer, "Interpretation of MIMO channel characteristics in rectangular tunnels from modal theory," *IEEE Transactions on Vehicular Technology*, vol. 57, no. 3, pp. 1974–1979, 2008.

[12] M. Liénard, P. Degauque, J. Baudet, and D. Degardin, "Investigation on MIMO channels in subway tunnels," *IEEE Journal on Selected Areas in Communications*, vol. 21, no. 3, pp. 332–339, 2003.

[13] M. Lienard and P. Degauque, "Propagation in wide tunnels at 2 GHz: a statistical analysis," *IEEE Transactions on Vehicular Technology*, vol. 47, no. 4, pp. 1322–1328, 1998.

[14] A. F. Molisch, "Ultrawideband propagation channels-theory, measurement, and modeling," *IEEE Transactions on Vehicular Technology*, vol. 54, no. 5, pp. 1528–1545, 2005.

[15] T. S. Rappaport, *Wireless Communications*, Prentice-Hall, Englewood Cliffs, NJ, USA, 1996.

[16] S. S. Ghassemzadeh, R. Jana, C. W. Rice, W. Turin, and V. Tarokh, "Measurement and modeling of an ultra-wide bandwidth indoor channel," *IEEE Transactions on Communications*, vol. 52, no. 10, pp. 1786–1796, 2004.

[17] J. Keignart and N. Daniele, "Channel sounding and modeling for indoor UWB communications," in *Proceedings of International Workshop on Ultra Wideband Systems (IWUWBS '03)*, Oulu, Finland, June 2003.

[18] D. Cassioli, M. Z. Win, and A. F. Molisch, "The ultra-wide bandwidth indoor channel: from statistical model to simulations," *IEEE Journal on Selected Areas in Communications*, vol. 20, no. 6, pp. 1247–1257, 2002.

[19] V. Hovinen, M. Hämäläinen, R. Tesi, L. Hentilä, and N. Laine, "A proposal for a selection of indoor UWB path loss model," Tech. Rep. IEEE P802.15-02/280-SG3a, Wisair, Tel Aviv, Israel, July 2002, http://grouper.ieee.org/groups/802/15/pub/2002/Jul02.

[20] A. Papoulis and S. U. Pillai, *Probability, Random Variables and Stochastic Processes*, McGraw-Hill, Boston, Mass, USA, 4th edition, 2002.

[21] J. P. Kermoal, L. Schumacher, K. I. Pedersen, P. E. Mogensen, and F. Frederiksen, "A stochastic MIMO radio channel model with experimental validation," *IEEE Journal on Selected Areas in Communications*, vol. 20, no. 6, pp. 1211–1226, 2002.

[22] G. J. Foschini and M. J. Gans, "On limits of wireless communications in a fading environment when using multiple antennas," *Wireless Personal Communications*, vol. 6, no. 3, pp. 311–335, 1998.